Geosci. Model Dev. Discuss., 4, 3313–3337, 2011
www.geosci-model-dev-discuss.net/4/3313/2011/
doi:10.5194/gmdd-4-3313-2011

Geoscientific Model Development Discussions

Supersaturation calculation in large eddy simulation models for prediction of the droplet number concentration

O. Thouron[1], **J.-L. Brenguier**[2], **and F. Burnet**[2]

[1]CNRS/CERFACS, URA1875, 42 avenue Gaspard Coriolis, 31057 Toulouse CEDEX 01, France
[2]CNRM/GAME, Meteo-France/CNRS-INSU, URA1357, 42 avenue Gaspard Coriolis, 31057 Toulouse CEDEX 01, France

Received: 24 October 2011 – Accepted: 18 November 2011 – Published: 5 December 2011

Correspondence to: O. Thouron (odile.thouron@cerfacs.fr)

Published by Copernicus Publications on behalf of the European Geosciences Union.

Abstract

A new parameterization scheme is described for calculation of supersaturation in LES models that specifically aims at the simulation of cloud condensation nuclei (CCN) activation and prediction of the droplet number concentration. The scheme is tested against current parameterizations in the framework of the Meso-NH LES model. It is shown that the saturation adjustment scheme based on parameterizations of CCN activation in a convective updraft over estimates the droplet concentration in the cloud core while it cannot simulate cloud top supersaturation production due to mixing between cloudy and clear air. A supersaturation diagnostic scheme mitigates these artefacts by accounting for the presence of already condensed water in the cloud core but it is too sensitive to supersaturation fluctuations at cloud top and produces spurious CCN activation during cloud top mixing. The proposed pseudo-prognostic scheme shows performance similar to the diagnostic one in the cloud core but significantly mitigates CCN activation at cloud top.

1 Introduction

Equivalent liquid potential temperature and the total water mixing ratio, r_t, are two conservative quantities in atmospheric numerical models. In a cloudy atmosphere, r_t is distributed onto water vapour and condensed water, either liquid or ice. This paper is focused on liquid water clouds, also referred to as warm clouds, and the liquid water mixing ratio is designated by r_c.

The water vapour mixing ratio, r_v, is thus equal to $r_t - r_c$ and the saturation water mixing ratio r_s can be derived from pressure and temperature as:

GMDD

4, 3313–3337, 2011

$$r_s(P,T) = \varepsilon \frac{e_s(T)}{P - e_s(T)} \quad (1)$$

where $e_s(T)$ is the saturation water vapour pressure over an infinite plane of pure water, T is the absolute temperature, and P is the pressure and ε is the ratio of the molecular weight of water vapor to dry air (Pruppacher and Klett, 1997).

The supersaturation, S, expresses the relative deviation of the water vapour mixing ratio with respect to its saturation value:

$$S = \left(\frac{r_v}{r_s} - 1 \right) \quad (2)$$

Supersaturation, which is currently expressed in % ($S \times 100$), rarely exceeds a few percents in warm clouds because there are generally enough cloud condensation nuclei and droplets to deplete water vapour excess. Consequently, adjustment to saturation is a good approximation, to within a few percents, for a diagnostic of the liquid water mixing ratio in warm clouds.

$$r_c = r_t - r_s \quad (3)$$

Calculation of supersaturation, however, is still required when the model also aims at predicting the number concentration of cloud droplets. Indeed, droplets form on cloud condensation nuclei, CCNs, that are hydrophilic, partly soluble particles at the surface of which the saturation water vapor pressure is lower than $e_s(T)$. Due to surface tension effects, however, the vapour pressure at the surface of a pure water particle increases when the particle size decreases. Because of this competition between solute and surface tension effects, the water vapour pressure at the surface of a particle exhibits a maximum when expressed as a function of the wet particle size. CCNs have to experience a supersaturation greater than this maximum to be activated as cloud droplets. Hence, a population of CCNs is currently represented by its activation spectrum $N_{act}(S)$ that establishes a direct link between the ambient supersaturation, S, and the number concentration of activated particles, N_{act}.

GMDD
4, 3313–3337, 2011

In summary, the calculation of supersaturation in a cloudy atmosphere is not necessary to derive the liquid water mixing ratio, as long as an uncertainty of a few percents is acceptable, but its peak value shall be determined when the model also aims at predicting the cloud droplet number concentration, N_c (Pruppacher and Klett, 1997).

Warm cloud microphysics schemes have thus been developed assuming saturation adjustment ($S = 0$) and using a diagnostic scheme for deriving the peak supersaturation (Twomey, 1959; Ghan et al., 1995; Cohard and Pinty, 1998). Such an approximation was quite satisfactory when the vertical resolution was greater than 100 m and the time steps longer than a few tens of seconds, which is currently how long it takes for supersaturation to increase at the base of a cloud updraft, reach its maximum, typically 50 m above the base, and fall down to its pseudo equilibrium value.

Today, LES models of cloud microphysics are ran with a vertical resolution of less than 10 m and time steps of less than 1 s. This is not fine enough for a complete prognostic calculation of supersaturation that requires time steps of milliseconds, typically, but this is too thin and too fast for assuming that supersaturation reaches and passes its maximum within a time step.

Consequently, new parameterizations have been developed to explicitly calculate supersaturation and simulate CCN activation and droplet condensation/evaporation. However, a numerical artefact currently happens at the interface between a cloud and its environment, when cloudy air is progressively advected in a clear grid box (Clark et al., 1973; Klassen and Clark, 1985; Grabowski, 1989; Grabowski and Smolarkiewicz, 1990; Kogan et al., 1995; Stevens et al., 1996; Grabowski and Morrison, 2008), for instance at the top of a stratoculumus layer. Indeed, explicit calculation of supersaturation is problematic because it is a second order variable compared to the model prognostic variables T and r_t. Small numerical errors in the advection scheme for instance can result in large fluctuations of the derived supersaturation. This artefact generates spurious supersaturation peak values, hence CCN activation and results in unrealistic N_c values at cloud top.

GMDD
4, 3313–3337, 2011

A new scheme is proposed here to reduce these artefacts. Parameterization schemes are briefly described in the next section, starting with the two commonly used techniques, adjustment to saturation (Sect. 2.1) and saturation diagnostic (Sect. 2.2), before describing the proposed approach in Sect. 2.3. The three schemes are then tested in a 3-D framework of an LES model (Sect. 3) to evaluate the benefits of the proposed parameterization.

2 Parameterization schemes

To simulate warm clouds including prediction of the cloud droplet number concentration, three prognostic variables are required beyond dynamics: the equivalent liquid water potential temperature θ_l or any thermodynamical variable conserved during condensation/evaporation processes, the total water mixing ratio r_t and the cloud droplet number concentration N_c. Note that additional variables are also required to simulate the formation of precipitation, such as the precipitating water mixing ratio and precipitating particle number concentration (Khairoutdinov and Kogan, 2000).

The parameterization schemes described in this section aim at the prediction of the cloud water mixing ratio r_c and of the number concentration of activated CCNs. A key issue is to avoid activation of already activated CCNs each time supersaturation is produced in a model grid box. This is only feasible if additional prognostic variables are used for describing the CCN population in the 3-D framework, including a sink term reflecting CCN activation.

When such a CCN scheme is not operational and the CCN population is assumed uniform over the whole domain, the problem can be partially addressed with only one additional prognostic variable. Indeed, beside advection, the cloud droplet number concentration increases when new CCNs are activated and decreases when droplets totally evaporate. At this stage, there is a direct correspondence between the activated CCN number concentration and the cloud droplet number concentration. The cloud droplet number concentration, however, also decreases when droplets collide, either

GMDD
4, 3313–3337, 2011

with other droplets (autoconversion) or with precipitating drops (accretion). The so called collection process is not conservative for the number concentration of activated CCNs. It is therefore common to use an additional prognostic variable N_{act} to represent the number concentration of activated CCNs (Cohard and Pinty, 1998). Like N_c, N_{act} is driven by CCN activation and droplet evaporation but it is not affected by the collection process.

2.1 Scheme A: adjustment to saturation with parameterized peak supersaturation

In this scheme, the cloud water mixing ratio is a diagnostic variable that is directly derived at each time step from total water, pressure and temperature Eq. (3), assuming no supersaturation. To diagnose the number concentration of activated CCNs, the supersaturation peak value, S_{max}, is derived from the time evolution equation of supersaturation in an ascending adiabatic volume of air, by setting the time derivative of supersaturation to 0 at the maximum:

$$\frac{dS}{dt} = \frac{1}{r_s}\frac{dr_v}{dt} - \frac{(S_{max}+1)}{r_s(P,T)}\frac{dr_s}{dt} = 0 \quad (4)$$

$\frac{dr_s}{dt} = \frac{dr_s}{dT}\frac{dT}{dt}$ expresses a forcing due to cooling by adiabatic ascent and $\frac{dr_v}{dt}$ expresses the sink of water vapour condensed on droplets that depends on the CCN spectrum. Various formulae have been derived to solve the system of differential equations using a parameterized description of the CCN activation spectrum (Leaitch et al., 1986; Ghan et al., 1995; Cohard et al., 1998; Abdul-Razzak and Ghan, 2000).

The diagnostic of maximum supersaturation, S_{max}, is directly translated into a diagnostic of activated CCN number concentration, N_{act}, using the CCN activation spectrum. To account for the non-reversibility of the activation process, N_{act} and N_c are updated each time the $N_{act}(S_{max})$ diagnosed value is higher than the current one.

Because the forcing is expressed as a function of vertical velocity only, these formulae are well suited for CCN activation at the base of convective clouds but they shall be

GMDD
4, 3313–3337, 2011

adapted when activation is mainly driven for instance by radiative cooling. A second limitation is that the formulae hold for grid boxes with no initial liquid water content, while any pre-existing condensed water in a model grid box significantly reduces the supersaturation peak value.

The main limitation though, is that the solution corresponds to the maximum supersaturation when the forcing is maintained until the maximum is reached. With a vertical velocity of the order of 1 m s^{-1} and a typical CCN distribution, the maximum is reached after a few tens of seconds while the convective cell as already travelled a few tens of meters. These formulae are therefore not suited for fine spatial and time resolution simulations of less than 10 m and 10 s, respectively.

2.2 Scheme B: diagnostic of supersaturation

With an additional prognostic variable, either r_v or r_c, it becomes possible to directly diagnose supersaturation. In a first step, supersaturation is derived from the values of the thermodynamical prognostic variables θ_l, r_t and r_c (or r_v) after advection and modification by processes other than condensation/evaporation, as:

$$S' = \frac{r_t - r_c - r_s}{r_s} \tag{5}$$

or

$$S' = \frac{r_v - r_s}{r_s} \tag{6}$$

This S' value is then used for both CCN activation (when $N_{CCN}(S') > N_{act}$) and droplet growth/evaporation using:

$$\frac{dr_c}{dt} = 4\pi\rho_w G S' I \tag{7}$$

where I is the integral radius of the droplet size distribution and $G = \frac{1}{F_K + F_D}$ where F_K is a function of thermal conductivity of the air and F_D is a function of the diffusivity of water

GMDD
4, 3313–3337, 2011

vapour (Pruppacher et Klett, 1997). The two conservative variables θ_l and r_t are not affected by condensation/evaporation, but the final value of r_c (or r_v) shall be updated according to Eq. (7).

The initial diagnostic of supersaturation provided by Eq. (6) is very sensitive to small errors in θ_l, r_t and r_c or r_v because it is a second order variable. Indeed, supersaturation rarely exceeds a few percents. The system is well buffered for condensation/evaporation since over(under)estimated supersaturation leads to an over(under)estimation of the condensation rate, so that, on average, r_c remains close to its optimal value. Spurious positive peak values of the supersaturation, however, have a significant impact on CCN activation because the process is non-reversible, hence producing unexpected high values of the cloud droplet number concentration.

2.3 Scheme C: pseudo-prognostic of supersaturation

The scheme proposed here aims at mitigating the weaknesses of the two approaches described above when the time step and vertical resolution of the model get shorter than 10 s and 10 m, respectively. A parameterization of the supersaturation peak value, such as the ones discussed in Sect. 2.1 is precluded because the peak value cannot be reached during so short time steps. Diagnostic of supersaturation is also precluded because it amplifies small errors in the advection of heat and moisture. The objective is also to derive an estimate of the supersaturation that combines both the forcing by the thermodynamics and the sink/source by condensation/evaporation of pre-existing droplets.

Like in Sect. 2.2, the scheme requires an additional prognostic variable for the condensate and a semi-prognostic variable to communicate the estimate of supersaturation from one time step to the next one, referred here to as S^t. The forcing term is derived from the values of the thermodynamical prognostic variables θ_l, r_t and r_c (or r_v) after advection and modification by processes other than condensation/evaporation, as:

GMDD
4, 3313–3337, 2011

$$\left(\frac{dS}{dt}\right)_f = \frac{S' - S}{\Delta t} \tag{8}$$

where Δt is the model time step and S' is calculated using Eq. (6) as in Sect. 2.2. The condensation/evaporation term $\left(\frac{dS}{dt}\right)_{ce}$ is derived as (see Appendix A):

$$\left(\frac{dS}{dt}\right)_{ce} = \left(1 + (S+1)\frac{L_v}{C_p}\frac{dr_s}{dT}\right)\frac{1}{r_s}\frac{dr_c}{dt} \tag{9}$$

where $\frac{dr_c}{dt}$ is calculated using S^t instead of S' in Eq. (7). The final value of supersaturation is then derived as:

$$S^{t+1} = S^t + \left(\left(\frac{dS}{dt}\right)_f + \left(\frac{dS}{dt}\right)_{ce}\right)\Delta t \tag{10}$$

S^t is used for CCN activation (when $N_{CCN}(S^1) > N_{act}$). S^{t+1} is stored for the next time step.

3 Tests in a 3-D framework

3.1 Model setup

To evaluate the three techniques discussed above, the Mesoscale Nonhydrostatic atmospheric research model (Meso-NH) is used. This model has been jointly developed by Météo-France Centre National de Recherches Meteorologiques (CNRM) and Laboratoire d'Aérologie, for large- to small-scale simulations of atmospheric phenomena. The dynamical core of the model (Lafore et al., 1998) is completed by a 3-D one-and-a-half turbulence scheme based on a prognostic equation of kinetic energy (Cuxart et al., 2000), with a Deardorff mixing length. Surface fluxes are computed using the Charnock's relation for roughness length (Charnock, 1955). Shortwave

GMDD
4, 3313–3337, 2011

and longwave radiative transfer calculations are performed following the European Centre for Medium-Range Weather Forecasts (ECMWF) Fouquart and Morcrette formulation (Morcrette, 1991). The model includes a two-moment bulk microphysical scheme based on the parameterization of Khairoutdinov and Kogan (2000), which was specifically, designed for LES studies of warm stratocumulus clouds (Geoffroy et al., 2008). A complete description of the model can be found online at http://www.aero.obs-mip.fr/mesonh/index2.html. This model has been extensively used for LES studies of boundary layer clouds, with the one moment and two moments microphysical schemes (Chosson, 2007; Geoffroy, 2008; Sandu, 2008, 2009).

The model is used here with a horizontal resolution of 50 m and a vertical resolution varying from 50 to 10 m, with the finest resolution in the cloud and at the inversion layer. Periodic boundary conditions are applied horizontally and the top of the domain is at 1.5 km. The time step is set to 1 s and the ECMWF radiation scheme is called every second in cloudy columns and every 120 s in clear columns. To avoid interactions between the cloud structures and the domain size, the horizontal domain dimension is set to 10 km for a 3-h simulation time run, following de De Roode et al. (2004). The prognostic variables are θ_l, r_t, r_c, and N_c.

The model initialisation fields originate from a non-precipitating stratocumulus cloud layer case that was observed on 9 July 1997, over the Northeast Atlantic, north of the Canary Islands, during the ACE-2 Cloudy Column experiment (Brenguier et al., 2000). The inversion layer was located at 960 m, with sharp jumps in both water vapour mixing ratio and liquid water equivalent temperature. To reduce the spin-up time, the simulations are performed with a sub-saturated initial profile and a cooling is applied during the first hour of simulation. The simulation is then continued for two more hours after cooling has been shutoff. Unlike the observed case, night time conditions are assumed.

To better evaluate the performance of the parameterizations and their sensitivity to entrainment-mixing processes, two simulations are performed with the same initialisation fields except for the values of the total water mixing ratio in the free troposphere

GMDD
4, 3313–3337, 2011

equal to 5 g kg^{-1} and 8 g kg^{-1}, respectively. These are thus referred to as the DRY and WET case.

3.2 General features

Figure 1 shows the vertical profiles of liquid water content, q_c, (top) and cloud droplet number concentration, N_c, (bottom) for the DRY (left) and WET (right) simulations. q_c, is used here instead of mixing ratio, r_c, to facilitate the comparison with in situ observations. The data represented by solid lines are averaged over the model cloudy columns (domain cloud fraction), while the dashed lines reflect values averaged over the cloudy grids in each model layer (layer cloud fraction) separately. Blue, black and red correspond to the "adjustment" or A, "diagnostic" or B, and "pseudo-prognostic" or C schemes, respectively.

The top row suggests that the schemes have no significant impact on the LWC profiles, although the A scheme exhibits a slightly greater and higher maximum in the DRY case. The DRY case also shows noticeable differences between the domain and layer cloud fraction averages that reflect the presence of clear air patches due to entrainment of very dry air from above the inversion.

In contrast, the cloud droplet concentration profiles (bottom) reveal that the A scheme significantly overestimates N_c. The dashed lines, that emphasize the differences at cloud base and top, where the layer cloud fraction is reduced, reveal that the overestimation starts at cloud base during activation of CCN in updraft.

The B and C schemes produce similar N_c predictions, except at cloud top where the B scheme starts overestimating the cloud droplet number concentration and generates N_c values as high as the A scheme in both the DRY and WET simulations. This feature reflects the final statement in Sect. 2.2 about the sensitivity of the diagnostic scheme to advection errors at the interface between cloudy and clear air.

GMDD
4, 3313–3337, 2011

3.3 CCN activation

To better understand these two specific features, widespread overestimation of cloud droplet number concentration from base to top with the A scheme and at the top only with the B scheme, it is useful to explore the activation process in depth. Figure 2 for the DRY case shows from top to bottom the results obtained with the A, B and C schemes, respectively. The left column is for the vertical distribution of supersaturation values in model grid boxes where CCN activation occurs. The middle column shows the number concentration of activated particles during the time step, and the right column represents the resulting number concentration of cloud droplets in all cloudy grid boxes. The far left graph shows the PDF of occurrence of activation events in the vertical, while the ones under each figure are for the PDF of parameter values. For comparison, the outcomes of the three schemes are superimposed in each PDF graph with the current one in bold.

This figure reveals that the A scheme produces supersaturation values greater than the two others and, at the middle of the cloud, values greater than at cloud base. This directly reflects the fact that the A scheme relies on a parameterization of the CCN activation process that only accounts for the vertical velocity and does not consider the sink term due to existing LWC. In contrast, the B and C schemes that account for the presence of LWC in a grid box generate lower supersaturation values, with greater ones at cloud base. Moreover, the A scheme also assumes that the supersaturation produced during a single time step lasts long enough for the CCN activation to be completed. Because supersaturation is a noisy parameter, the chances to activate large concentrations of CCN each time it reaches its maximum are significantly increased. In contrast, the B and C schemes progressively activate small amount of CCN ($< 40\,cm^{-3}$), as simulated for instancewhen using a high resolution explicit supersaturation scheme in a 1-D framework, although both schemes build up cloud droplet number concentration values of about $150\,cm^{-3}$ and a few values greater than $200\,cm^{-3}$.

GMDD
4, 3313–3337, 2011

There is however a noticeable difference between the B and C schemes, namely that the B scheme only produces spurious peak values of supersaturation at cloud top, hence spurious activation of new CCNs and spurious values of cloud droplet number concentration at cloud top. These high concentrations of activated CCNs are reflected in the corresponding PDF (middle column) that shows similar probabilities of high concentrations of activated CCNs for the A and B schemes (black and blue curves) while such occurrences fall below 10^{-4} with the C scheme (red curve) when the concentration of activated CCNs becomes greater than $60\,cm^{-3}$.

In summary, this figure shows that, compared to the adjustment scheme (A), the diagnostic of supersaturation (B scheme) is efficient at simulating the progressive CCN activation at cloud base and the buffering of the supersaturation production in the cloud core due to existing LWC. It, however, reveals that the B scheme remains too sensitive to peak supersaturation artefacts due to advection at the interface between cloudy and clear air, mainly at cloud top.

Figure 3 is similar to Figure 2 for the WET case. As shown in Fig. 1, the WET case has a more homogeneous cloud fraction (the domain and layer cloud fraction LWC averages are similar from base to top) than the DRY case, suggesting that the moister entrained air produces less clear air patches within the cloud layer. As a result, the three schemes do not generate anymore CCN activation in the middle of the cloud layer, but the A scheme still significantly overestimates the cloud droplet number concentration at cloud base. Spurious CCN activation at cloud top is noticeable with the three schemes, although less pronounced with the C scheme. This figure illustrates the intrinsic limitations of an LES model (spatial and time resolutions) compared to Lagrangian simulations of the activation process, but still demonstrates that the pseudo-prognostic approach efficiently mitigates the main activation artefacts of Eulerian models.

Figure 4 aims at illustrating how supersaturation is generated in a 3-D framework. For the A (top), B (middle) and C (bottom) schemes and the DRY (left) and WET (right) cases, the figure shows the supersaturation values in each grid box plotted against the

GMDD
4, 3313–3337, 2011

vertical velocity, The PDF of the parameters are indicated on the left and under each graph. The colour scale corresponds to the liquid water mixing ratio in the grid box.

The top row directly reflects the A scheme parameterization of supersaturation as a function of vertical velocity that does not account for the presence of liquid water in the grid box. In contrast, both the middle and bottom row attest that the B and C schemes only produce high values of supersaturation when the liquid water mixing ratio is reduced.

Interestingly, the B and C schemes generate extreme positive and negative values of supersaturation in grid boxes with vertical velocities close to 0. This feature reflects the production of supersaturation when cloudy air is mixed with dry air (concavity of the Clausius-Clapeyron curve). However, to our knowledge, peak values of the cloud droplet number concentration at cloud top have never been reported from in situ measurements. Our interpretation is that such values of supersaturation are due to the still coarse spatial resolution of the model, while in real cloud the competition between mixing of entrained dry air and droplet evaporation down to the smallest scales rather results in a decrease of the cloud droplet number concentration at constant droplet diameter, a feature commonly referred to as inhomogeneous mixing.

3.4 Microphysical impact of entrainment-mixing

The covariance of liquid water mixing ratio and cloud droplet number concentration provides an additional framework to further evaluate how realistic the simulations are. The technique has been extensively used to analyze in situ measurements of cloud microphysics (Burnet and Brenguier, 2007). Each measured sample is characterized by the cloud droplet number concentration and the mean volume radius (to the cube), r_v^3, of the droplet size distribution:

$$r_v^3 = \frac{3q_c}{4\pi\rho_w N_c} \tag{11}$$

GMDD
4, 3313–3337, 2011

Both values are then normalised by their adiabatic values at the sample altitude level to correct the impact of fluctuations of the sample altitude above cloud base (see Burnet and Brenguier, 2007, for more details on the methodology). This methodology is illustrated in Fig. 5 with the grid box values from the upper 100 m of the cloud layer, as represented in Fig. 1 by the two green bars. The hyperboles represent values of the LWC adiabatic ratio (q_c/q_{cad}) from 1 for adiabatic samples (solid curve), down to 10 % (dashed curves) and the thick dashed line in each panel shows the limit for pure homogeneous mixing. Indeed, when an adiabatic cloud volume is mixed with pure environmental air characterized here by a water mixing ratio of 5 and 8 g m^{-3} for the DRY (left column) and WET (right) case, respectively, the results must lay to the left of the homogeneous mixing limit. The colour scale corresponds to the vertical velocity in the grid box.

Obviously the adjustment scheme (top row) produces features that are different from the two other schemes and also different from in situ observations as reported in Burnet and Brenguier (2007). First, adiabatic values are grouped around the 1/1 coordinates, while fluctuations of vertical velocity during CCN activation generally leads to a noticeable variability of the adiabatic cloud droplet number concentration. This is nicely simulated with the two other schemes (middle and bottom rows), as shown by the dispersion of the normalized values along the adiabatic LWC isoline (solid curve). This corroborates again the fact that the adjustment scheme activates everywhere in the cloud layer the same number concentration of CCNs that corresponds to peak values of the supersaturation.

The most unrealistic feature, though, is the stratification of the cloud droplet number concentration dilution ratio (N_c/N_{ad}) with the vertical velocity and the presence of superadiabatic droplet sizes (normalized droplet sizes greater than 1 on the Y axis). These two features reflect the limitations of the adjustment scheme that only activate CCNs when the vertical velocity is positive. When cloudy air is mixed with dry air, the cloud droplet number concentration is diluted and supersaturation can be produced by the mixture of the two air masses, hence leading to activation of new CCNs, even the

GMDD
4, 3313–3337, 2011

vertical velocity is close to 0, or even negative. The adjustment scheme that requires a positive velocity, is unable to activate new CCNs and condenses the supersaturated water vapour onto the remaining droplets hence leading to super adiabatic growth.

For these two reasons, the adjustment scheme is not recommended for fine resolution LES simulations when the objective is to realistically simulate CCNs activation and entrainment-mixing processes impacts on cloud microphysics.

The B and C scheme show quite similar results, but one can notice the occurrence of superadiabatic cloud droplet number concentration (to the right of the homogeneous mixing limit) when using the B scheme (middle row). These unrealistic values of the cloud droplet number concentration after mixing are due to spurious CCN activation already discussed in the previous section.

The C scheme is more robust with only very few cases of spurious CCN activation after mixing, and realistic N_c, r_v^3 and vertical velocity distributions.

4 Conclusions

Three parameterizations of supersaturation and CCN activation have been tested here in the framework of a 3-D LES model that aims at predicting both LWC and the cloud droplet number concentration in convective clouds.

The first one assumes no supersaturation and the liquid water mixing ratio is exactly equal to the difference between the total mixing ratio and the saturated one. For CCN activation, a peak value of supersaturation is diagnosed at each time step based on a formula that involves the vertical velocity in the grid box as a forcing term and a parameterized description of the CCN activation spectrum, assuming (i) the conditions last long enough for the supersaturation to reach its maximum and (ii) the grid box is initially void of droplets.

The various tests demonstrate that such a parameterization is not effective when the vertical resolution and the time steps are much shorter than what is necessary for (i) to be valid. Moreover (ii) is obviously not fulfilled within the cloud core after

GMDD
4, 3313–3337, 2011

CCN activation is completed and droplets have grown enough. Consequently, the scheme keeps activating new CCNs in the cloud core while explicit calculations of the supersaturation would suggest the opposite. Finally, at cloud top, the scheme is unable to diagnose production of supersaturation by mixing because the vertical velocity is mostly null or negative. Consequently, it condenses the surplus of water vapour onto a diluted population of droplets that progressively develop superadiabatic unrealistic sizes.

The second scheme involves an additional variable to keep track of the condensed water. An intermediate value of supersaturation is diagnosed from the temperature, total and liquid water mixing ratios after advection and processes other than microphysics. This value is then used for CCN activation and condensational droplet growth. Because condensed water is accounted for in the diagnostic of supersaturation this scheme avoids the main limitations of the previous one and it ralistically simulate the variability of cloud droplet number concentration due to the variability of vertical velocity during the activation process. It also simulates supersaturation production by mixing at cloud top but it is slightly to sensitive to small errors in the advection scheme and significantly overestimates CCN activation at the top.

The third scheme builds up upon the benefits of the second one, but also add a pseudo prognostic of the supersaturation based on approximations of the source and sink terms. Introducing the dependence on the time step by integrating the time evolution of supersaturation, this scheme smoothes out spurious fluctuations of temperature and water mixing ratios, hence of the supersaturation and produces more realistic values of the cloud droplet number concentration at cloud top.

It is therefore recommended to use such an improved scheme when the spatial and time resolutions of the model are shorter than 50 m and 10 s, respectively, and when the objective is to realistically simulate CCN activation droplet growth and the impact of mixing. Note, however, that mixing is assumed to be homogeneous and the scheme is unable to replicate the inhomogeous mixing features that are currently observed in stratocumulus clouds.

GMDD
4, 3313–3337, 2011

Appendix A

Condensation/evaporation forcing term for the supersaturation

The equation for the time evolution of the supersaturation is derived from Eq. (2) as:

$$\frac{dS}{dt} = \frac{1}{r_s}\frac{dr_v}{dt} - \frac{(S+1)}{r_s}\frac{dr_s}{dt} \tag{A1}$$

When only water phase changes are considered:

$$\frac{dr_v}{dt} = -\frac{dr_c}{dt} \tag{A2}$$

and

$$\frac{dr_s}{dt} = \frac{dr_s}{dT}\frac{dT}{dt} = \frac{dr_s}{dT}\frac{L_v}{C_p}\frac{dr_s}{dt} \tag{A3}$$

where L_v and C_p are the latent heat of condensation and the specific heat at constant pressure.

A3 leads to Eq (9).

Acknowledgements. This work has been partly funded by EUCAARI (European Integrated project on Aerosol Cloud Climate and Air Quality interactions) No. 036833-2.

References

Abdul-Razzak, H. and Ghan, S. J: A parameterization of aerosol activation 2. Multiple aerosol types, J. Geophys. Res., 105(D5), 6837–6844, 2000.

Clark, T. L.: Numerical modeling of the dynamics and microphysics of warm cumulus convection, J. Atmos. Sci., 30, 857–878, 1973.

Brenguier, J. L., Chang, P. Y., Fouquart, Y., Johnson, D. W., Parol, F., Pawlowska, H., Pelon, J., Schueller, F., and Snider, J.: An overview of the ACE-2 CLOUDYCLOUMN closure experiment, Tellus B, 52, 815–927, 2000

GMDD

4, 3313–3337, 2011

Burnet, F. and Brenguier, J. L.: Observational study of the entrainment mixing process in warm convective clouds. J. Atmos. Sci., 64, 1995–2011, 2007.
Charnock, H.: Wind stress over a water surface, Q. J. Roy. Meteor. Soc., 81, 639–640, 1955.
Chosson, F., Brenguier, J. L., and Schüller, L.: Entrainment mixing and radiative transfer simulation in boundary layer clouds, J. Atmos. Sci., 64, 2670–2682, 2007
Cohard, J., Pinty, J., and Bedos, C.: Extending twomey's analitical estimate of nucleated cloud droplet concentration from CCN spectra, J. Atmos. Sci., 55, 3348–3357, 1998.
Cuxart, J., Bougeault, P., and Redelsperger, J. L.: A turbulence scheme allowing for mesosacle and large eddy simulation, Q. J. Roy. Meteor. Soc., 126, 1–30, 2000.
De Roode, S. R., Duynkerke, P. G., and Jonker, H. J. J: Large-eddy simulation: How large is large enough?, J. Atmos. Sci., 61, 403–421, 2004.
Ghan, S. J., Chuang, C. C., Easter, R. C., and Penner, J. E.: A parameterization of cloud droplet nucleation. Part II: Multiple aerosol types, Atmos. Res., 36, 39–54, 1995.
Geoffroy, O., Brenguier, J.-L., and Sandu, I.: Relationship between drizzle rate, liquid water path and droplet concentration at the scale of a stratocumulus cloud system, Atmos. Chem. Phys., 8, 4641–4654, doi:10.5194/acp-8-4641-2008, 2008.
Grabowski, W. W.: Numerical experiments on the dynamics of the cloud-environment interface: small cumulus in a shearfree environment, J. Atmos. Sci., 46, 3513–3541, 1989.
Grabowski, W. W. and Morrison, H.: Toward the mitigation of spurious cloud-edge supersaturation in cloud models, Mon. Weather Rev., 136, 1224–1234, 2008.
Grabowski, W. W. and Smolarkiewicz, P. K.: Monotone finite difference approximations to the advection-condensation problem, Mon. Weather Rev., 118, 2082–2097, 1990.
Khairoutdinov, M. and Kogan, Y.: A new cloud physics parameterization in a large-eddy simulation model of marine stratocumulus, Mon. Weather Rev., 128, 229–243, 2000.
Klaassen, G. P. and Clark, T. L.: Dynamics of the cloud environment interface and entrainment in small cumuli: twodimensional simulations in the absence of ambient shear, J. Atmos. Sci., 42, 2621–2642, 1985.
Kogan, Y. L., Khairoutdinov, M. P., Lilly, D. K., Kogan, Z. N., and Liu, Q.: Modeling of stratocumulus cloud layers in a large eddy simulation model with explicit microphysics, J. Atmos. Sci., 52, 2923–2940, 1995
Lafore, J. P., Stein, J., Asencio, N., Bougeault, P., Ducrocq, V., Duron, J., Fischer, C., Héreil, P., Mascart, P., Masson, V., Pinty, J. P., Redelsperger, J. L., Richard, E., and Vilà-Guerau de Arellano, J.: The Meso-NH Atmospheric Simulation System. Part I: adiabatic

GMDD
4, 3313–3337, 2011

formulation and control simulations, Ann. Geophys., 16, 90–109, doi:10.1007/s00585-997-0090-6, 1998.
Leaitch, W. R., Strapp, J. W., Isaac, G. A., and Hudson, J. G.: Cloud droplet nucleation and cloud scavenging of aerosol sulphate in polluted atmopheres, Tellus B, 38, 328–344, 1986
Morcrette, J. J.: Radiation and cloud radiative properties in the ECMWF operational weather forecast model, J. Geophys. Res., 96D, 9121–9132, 1991.
Pruppacher, H. R.and Klett, J. D.: Microphysics of Clouds and Precipitation, 2nd Edn., Kluwer Academic Publishers, Dordrecht, The Netherlands, 954 pp., 1997.
Stevens, B., Walko, R. L., and Cotton, W. R.: The spurious production of cloud-edge supersaturation by Eulerian models, Mon. Weather Rev., 124, 1034–1041, 1996.
Sandu, I., Brenguier, J. L., Geoffroy, O., Thouron, O., and Masson, V.: Aerosol impacts on the diurnal cycle of marine stratocumulus, J. Atmos. Sci., 65, 2705–2718, 2008.
Sandu, I., Brenguier, J.-L., Thouron, O., and Stevens, B.: How important is the vertical structure for the representation of aerosol impacts on the diurnal cycle of marine stratocumulus?, Atmos. Chem. Phys., 9, 4039–4052, doi:10.5194/acp-9-4039-2009, 2009.
Twomey, S.: The nuclei of natural cloud formation. Part II: The supersaturation in natural clouds and the variation of cloud droplet concentration, Pure Appl. Geophys., 43, 243–249, 1959.

GMDD
4, 3313–3337, 2011

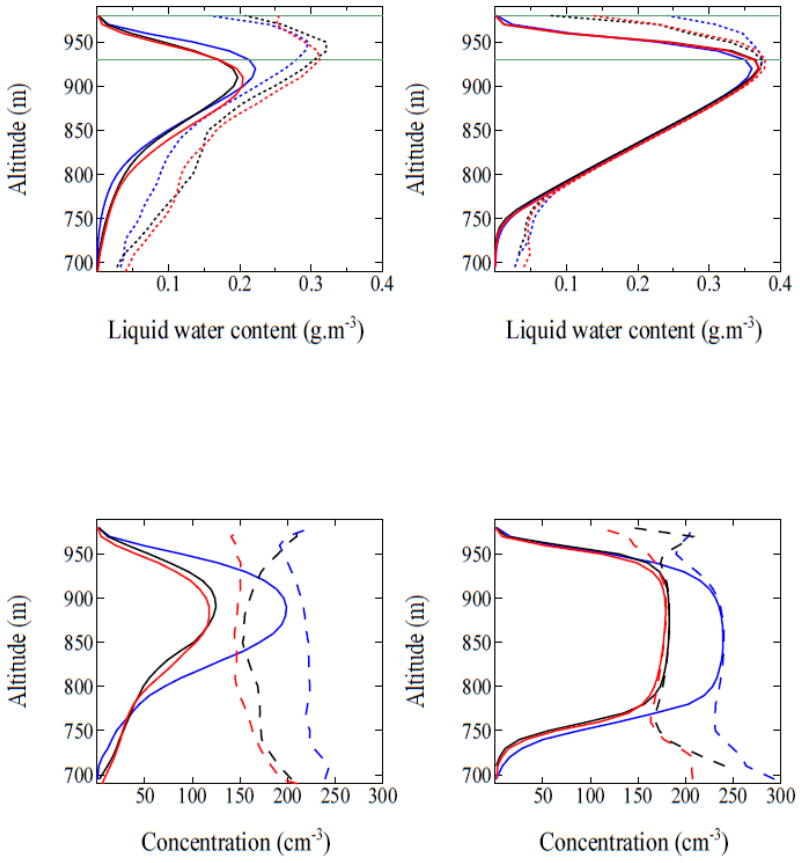

Fig. 1. Vertical profiles of LWC (top) and cloud droplet number concentration (bottom) averaged over the simulation domain cloud fraction (solid line) and over each layer cloud fraction (dashed line) for the DRY (left) and WET (right) case. Blue, black and red correspond to the "adjustment" or A, "diagnostic" or B, and "pseudo-prognostic" or C schemes, respectively.

GMDD
4, 3313–3337, 2011

Supersaturation calculation in large eddy simulation models

O. Thouron et al.

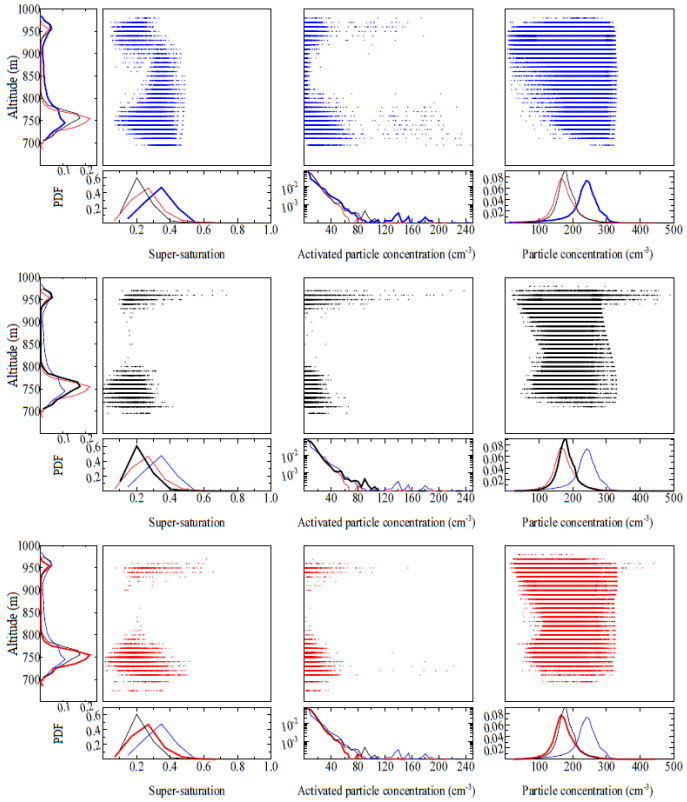

Fig. 2. For the DRY case: vertical distribution of supersaturation values in model grid boxes where CCN activation occurs (left), number concentration of activated particles, N_{act}, during the time step (middle) and resulting number concentration of cloud droplets, N_c, in all cloudy grid boxes (right) with the A (top-blue) , B (middle line-black) and C (bottom-red) schemes. The far left graph shows the PDF of occurrence of activation events in the vertical, while the ones under each figure are for the PDF of parameter values.

GMDD
4, 3313–3337, 2011

Supersaturation calculation in large eddy simulation models

O. Thouron et al.

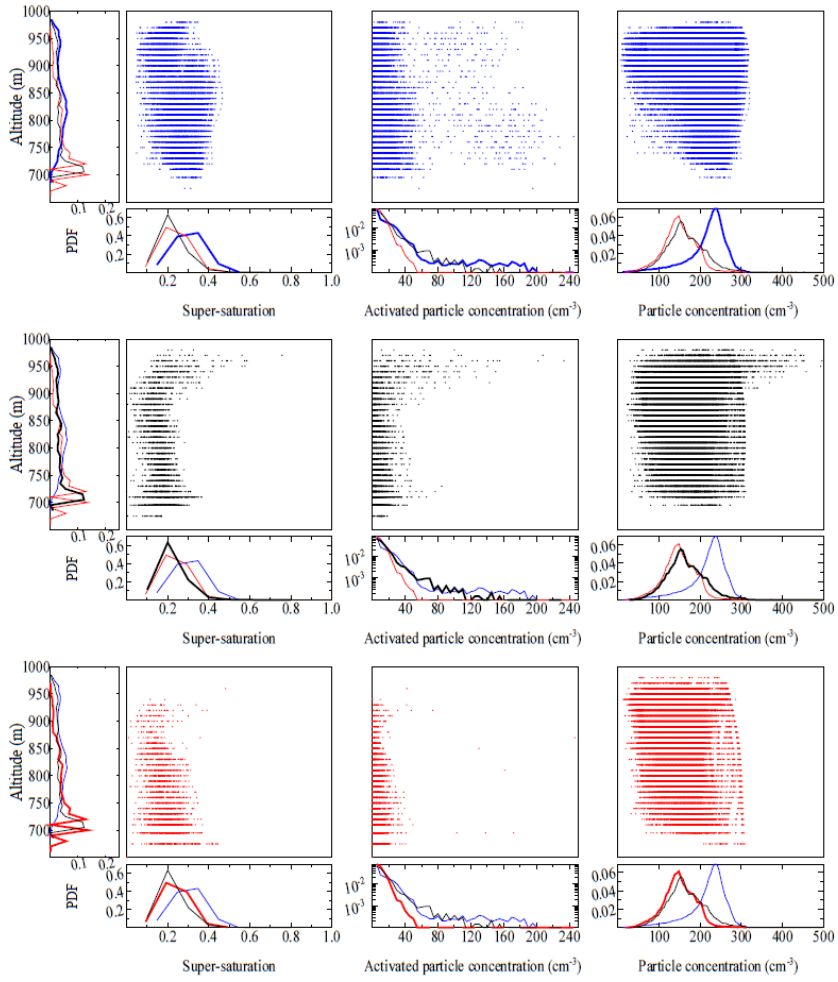

Fig. 3. Same as Fig. 2 for the WET case.

GMDD
4, 3313–3337, 2011

Supersaturation calculation in large eddy simulation models

O. Thouron et al.

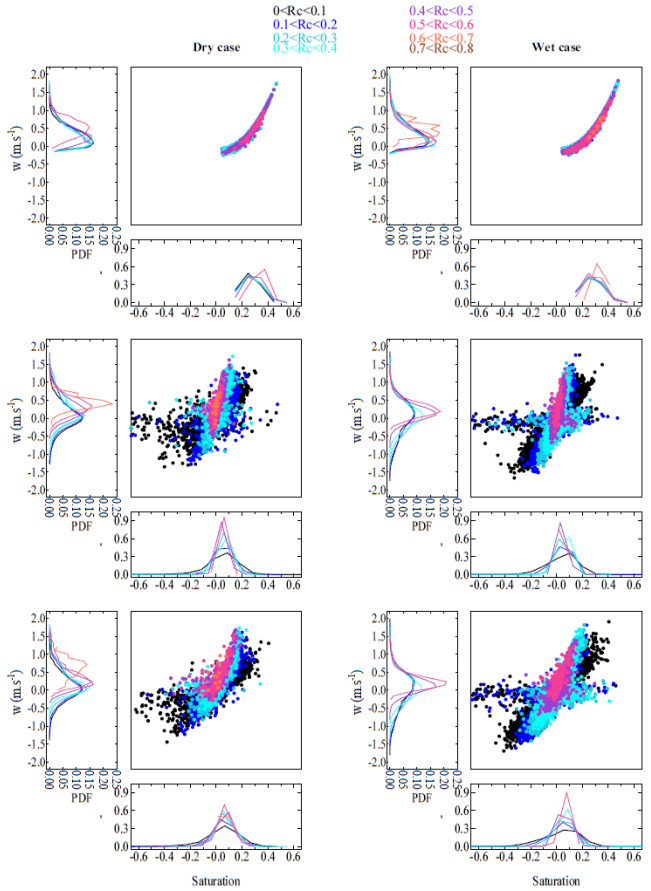

Fig. 4. Supersaturation as a function of vertical velocity for the A (top), B (middle) and C (bottom) schemes and the DRY (left) and WET (right) cases. The PDF of the parameters are indicated on the left and under each graph. The colour scale corresponds to the liquid water mixing ratio in the grid box.

GMDD
4, 3313–3337, 2011

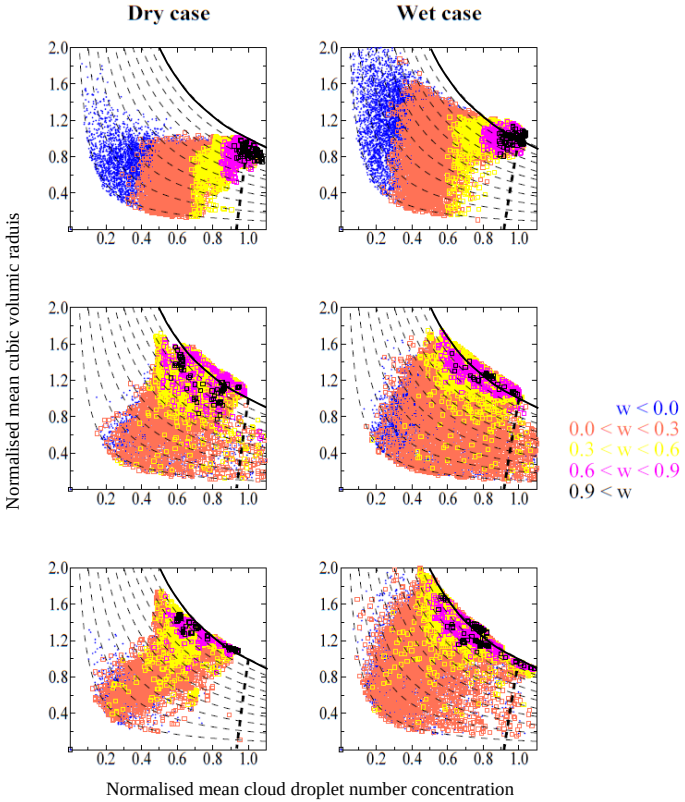

Fig. 5. Normalised mean cubic volume radius as a function of the normalised mean cloud droplet number concentration from the upper 100 m of the cloud layer for the DRY (left) and the WET (right) cases. Solid and dashed lines represent values of the LWC dilution ratio (q_c/q_{cad}) from 1 for adiabatic samples (solid curve), down to 10 % (dashed curves). Thick dashed line shows the limit for pure homogeneous mixing. The colour scale corresponds to the vertical velocity in the grid box.

GMDD
4, 3313–3337, 2011